Flexible, charged biopolymers in monovalent and mixed-valence salt: Regimes of anomalous electrostatic stiffening and of salt insensitivity

Sarah N. Innes-Gold

Materials Dept., University of California, Santa Barbara, USA

David R. Jacobson

Physics Dept., University of California, Santa Barbara, USA and

Current Affiliation: JILA, National Institute of Standards and

Technology and University of Colorado, Boulder, Colorado

Philip A. Pincus

Materials Dept. and Physics Dept.,

University of California, Santa Barbara, USA

Mark J. Stevens

Center for Integrated Nanotechnologies,

Sandia National Laboratories, Albuquerque, USA

Omar A. Saleh

Materials Dept. and Biomolecular Science and Engineering Program,

*University of California, Santa Barbara, USA**

(Dated: June 18, 2021)

Abstract

The conformations of biological polyelectrolytes (PEs), such as polysaccharides, proteins, and nucleic acids, affect how they behave and interact with other biomolecules. Relative to neutral polymers, PEs in solution are more locally rigid due to intra-chain electrostatic repulsion, the magnitude of which depends on the concentration of added salt. This is typically quantified using the Odijk-Skolnick-Fixman (OSF) electrostatic-stiffening model, in which salt-dependent Debye-Hückel (DH) screening modulates intra-chain repulsion. However, the applicability of this approach to flexible PEs has long been questioned. To investigate this, we use high-precision single-molecule elasticity measurements to infer the scaling with salt of the local stiffness of three flexible biopolymers (hyaluronic acid, single-stranded RNA, and single-stranded DNA) in both monovalent and mixed-valence salt solutions.

In monovalent salt, we collapse the data across all three polymers by accounting for charge spacing, and find a common power-law scaling of the electrostatic persistence length with ionic strength with an exponent of 0.66 ± 0.02. This result rules out simple OSF pictures of electrostatic stiffening. It is roughly compatible with a modified OSF picture developed by Netz and Orland; alternatively, we posit the exponent can be explained if the relevant electrostatic screening length is the inter-ion spacing rather than the DH length.

In mixed salt solutions, we find a regime where adding monovalent salt, in the presence of multivalent salt, does not affect PE stiffness. Using coarse-grained simulations, and a three-state model of condensed, chain-proximate, and bulk ions, we attribute this regime to a "jacket" of ions surrounding the PE that regulates the chain's effective charge density as ionic strength varies. The size of this jacket in simulations is again consistent with a screening length controlled by inter-ion spacing rather than the DH length. Taken together, our results describe a unified picture of the electrostatic stiffness of polyelectrolytes in the mixed-valence salt conditions of direct relevance to cellular and intercellular biological systems.

* saleh@ucsb.edu

I. INTRODUCTION

Polyelectrolytes (PEs) are polymers with ionizable groups, becoming charged in aqueous solution. They have diverse applications, including in processing oil and concrete, as food additives, and in biomedical tools [1]. Natural polyelectrolytes feature prominently in biology, as most biological macromolecules are charged. Interactions between charges control the behavior of PE systems and are sensitive to the amount of salt present in solution. As salt is added, inter-charge repulsion is screened, reducing the PE stiffness. The salt-dependent electrostatic stiffness is often modeled as an additive term to the chain's intrinsic molecular persistence length l_p^0, giving a total persistence length $l_p = l_p^0 + l_p^{elec}$ [2]. Much prior work has been devoted to how l_p^{elec} should scale with ionic strength I [3]. One such theory is that of Odijk [2], and Skolnick and Fixman [4] (OSF). They calculate the increase in bending energy of a semiflexible polymer due to charges that interact via a screened Coulomb potential. The resulting expression is:

$$l_p^{elec} = \frac{l_B}{4\kappa^2 d^2} \quad \text{(OSF)} \tag{1}$$

where d is the PE charge spacing, $l_B = \frac{e^2}{4\pi\epsilon\epsilon_0 k_B T}$ is the Bjerrum length, with elementary charge e, vacuum permittivity ϵ, dielectric constant ϵ_0, and thermal energy $k_B T$, and κ^{-1} is the electrostatic screening length. Typically, the Debye-Hückel (DH) screening length, $\kappa_{DH}^{-1} = \sqrt{8\pi l_B I}$, is used, where ionic strength I depends on the concentration c and valence (charge) Z of all ion species i, through $I = \frac{1}{2}\sum_i c_i Z_i^2$. Equation 1 predicts l_p^{elec} scales with κ_{DH}^{-2} or I^{-1}. OSF theory is frequently used due to its simple analytical expression, and some have found double-stranded DNA (dsDNA) elasticity data in agreement with the OSF prediction [5]. However, many other studies show disagreement with the OSF prediction, including data on dsDNA [6–8], single-stranded nucleic acids (ssNAs) [9–13], and hyaluronic acid (HA) [14]. Barrat and Joanny (BJ) revisited the OSF picture, incorporating fluctuation effects to make the model more appropriate for flexible chains [15]. The BJ calculation predicts that for flexible chains, l_p^{elec} scales with κ_{DH}^{-1}, or $I^{-1/2}$. Experiments on flexible synthetic chains [16], ssDNA [9–11, 13] and ssRNA [12] have shown results consistent with this exponent.

The mean-field and weak potential assumptions of DH theory are not appropriate for treating multivalent ions, which interact strongly with charged chains [17]. For highly

charged chains, such as dsDNA, even interactions with monovalent ions can be strong. These cases are better treated with condensation theories. The approach of condensation theories is to predict renormalized chain charge spacing d_{eff}, which can be substituted for the structural charge spacing d when calculating electrostatic persistence length (e.g. when using Equation 1) [15]. The best-known theory of counterion condensation is that of Manning [18] and Oosawa [19]. It considers a cylindrical PE with no added salt, and is applicable when the Debye length is very long compared to the PE charge spacing, predicting $d_{eff} = Zl_B$ where Z is the counterion valence [20]. However, since counterion condensation is an electrostatic phenomenon, it is clear that it will in general be affected by the amount of salt added to solution.

Some theoretical work has considered how the presence of monovalent salt affects condensation of multivalent ions on PEs. One approach is to use two-state models (bound and free ions) that incorporate bulk salt through Debye screening [21, 22], showing, as one might expect, that added 1:1 salt weakens condensation. Dobrynin further expanded upon Manning-Oosawa theory to explore how counterion condensation will affect the rigidity of a semiflexible polymer [23]. This theory predicts that in monovalent salt $l_p^{elec} \sim I^{-0.5}$ with further logarithmic corrections for fluctuations. Other work has extended condensation models beyond Debye screening by applying nonlinear Poisson-Boltzmann calculations [24, 25], and by considering the effect of counterion fluctuations [26]. Many others have made theoretical contributions to the field, including investigations of condensation on flexible PEs [27] and the chain collapse that can result from it [28, 29].

A variety of experiments support the idea that counterions condense onto PEs and modify their charge. Counterion condensation has been shown for dsDNA using NMR [30, 31], and collapse and aggregation of dsDNA in the presence of multivalent cations has been attributed to ion condensation [5, 22]. Models of ssNA force-extension curves which treat charge spacing as a free parameter were successful in fitting experimental data in 1:1 salt, and found fit charge spacing values larger than the structural spacing [32, 33], also supporting monovalent condensation. However, a systematic understanding of how multivalent condensation on PEs is affected by bulk non-condensing salt is still lacking. In our prior publication [34], we reported a phenomenon wherein HA's stiffness becomes insensitive to changes in I when a small constant amount of 3:1 salt is added. To our knowledge, this salt-insensitive regime had not previously been reported, and we attribute it to a salt-dependent condensation

phenomenon, suggesting it should occur generally for flexible PEs in salt mixtures.

Following the results of our prior publication, we now present a thorough investigation of ionic strength dependent PE stiffness in monovalent and mixed valence salt solutions. We conduct single-molecule magnetic tweezers experiments that extract estimates of l_p^{elec} from measurements of extension L vs. applied force f of three flexible charged biopolymers: HA, ssDNA, and ssRNA. We find that in monovalent salt, l_p^{elec} scales as a 0.66 ± 0.02 power law with ionic strength for all three PEs (Section III A). A similar exponent was predicted by Netz and Orland [35], attributed to condensation of monovalent ions, though we discuss an alternate explanation below. We next conduct experiments on HA and ssDNA in the presence of multivalent ions and show that a multivalent-induced I-insensitive regime of chain stiffness occurs in two chemically distinct systems (Section III B). The effect is also demonstrated in coarse-grained molecular dynamics simulation on HA-like and ssNA-like bead-spring chains (Section IV). Upon analyzing the microscopic details of the simulation, we find an 'ion-jacket' region in the vicinity of the PE in which an exchange process occurs: as total monovalent salt concentration increases, the singly-charged ions replace multivalent ions near the chain, reducing ion condensation while increasing the local ionic strength. We investigate this phenomenon using an analytical three-state model that invokes a Donnan equilibrium to explore the jacket's ionic environment (Section V); this analysis corroborates a trade-off between weakening condensation and increasing local ionic strength. We posit this phenomenon regulates the effective charge density of the PEs, and thus their conformation, in varying ionic conditions. Overall, our results use a multi-faceted approach, including experiment, simulation, and theory, to demonstrate a somewhat unexpected unity in the behavior of chemically-distinct PEs, marked by control of conformation through a non-OSF exponent and an effective charge spacing, with the latter sensitive to complex condensation phenomena.

II. METHODS

A. Magnetic Tweezers Experiments

To investigate PE behavior, we perform experiments on three different biopolymers: hyaluronic acid (HA), with intrinsic persistence length $l_p^0 \approx 5$ nm [14, 36] and charge spac-

ing $d = 1$ nm, single-stranded DNA (ssDNA), with $l_p^0 < 1$ nm and $d = 0.7$ nm [37], and single-stranded RNA (ssRNA) with $l_p^0 < 1$ nm and $d = 0.6$ nm [37].

To obtain ssDNA, a segment of lambda-phage double-stranded DNA (10.5 kbp) functionalized with thiol and biotin groups was synthesized by polymerase chain reaction with biotin and thiol primers (IDT), purified with a PCR cleanup kit (Zymo Research), and thermally and chemically denatured with glyoxal, following Ref. [11]. Hyaluronic acid (2.5 MDa), modified to allow chemical tethering to two surfaces, was purchased from Creative PEGworks. Each HA chain has a biotin group at the reducing end, and thiol groups at random locations internal to the chain, with a stoichiometry of one thiol per chain. Poly(U) ssRNA was synthesized as in Ref. [12] by elongation of 20-bp 5'-thiol labeled poly(U) primers using polynucleotide phosphorylase from E. coli (Sigma-Aldrich) under the reaction conditions of Ref. [38]. The resulting approximately 4,000–10,000 nucleotide chains were 3'-labeled with biotin by incorporation of biotin-dUTP using terminal deoxynucleotidyl transferase (Life Technologies). The HA attachment strategy unavoidably leads to polydispersity in tether length, as does the ssRNA synthesis, necessitating normalization by contour length in both cases.

Microfluidic sample chambers were constructed using maleimide-functionalized PEG-grafted glass surfaces purchased from Microsurfaces, Inc. The attachment of the thiol (and associated chain) to the maleimide surface was carried out in 50 mM sodium phosphate buffer (pH 7.2), 50 mM NaCl, 0.03% Tween-20, and 100 mM TCEP. After attachment, excess polymer was removed by rinsing with 10 mM MOPS buffer (pH 7). The biotin-labeled ends of the chains were then attached to 1 μm MyOne C1 streptavidin-coated paramagnetic beads (Invitrogen), and unbound beads were rinsed away. To ensure each bead is attached to only one polymer, the tether length is tracked as the magnets (and bead) are rotated. Multiple tethers become interwound during rotation, decreasing the bead height [39].

All experiments include a small amount of monovalent buffer: 1-10 MOPS (pH 7) or 10 mM Tris HCl (pH 7.5). Under these conditions, MOPS contributes an ionic strength equal to 40% of its concentration, and Tris contributes 70%.

The flow cell containing tethers was placed into a custom-built magnetic tweezers instrument. The design of this instrument follows principles described previously [40]: A force is applied to the magnetic beads by application of an adjustable magnetic field gradient. The force is calibrated for each tether by recording the bead's thermal fluctuations and applying

a Langevin analysis [41]. Tether extension is measured through optical tracking of the magnetic bead [40, 42]. In the present instrument, optical tracking is accomplished by imaging the bead at 400 Hz onto a EoSens 3CXP high-speed CMOS camera from Mikrotron, with videos streamed in real-time to a computer using the BitFlow Cyton-CXP4 framegrabber, and analyzed to find 3-D bead position using previously described GPU code [43].

B. Simulations

We conducted coarse-grained molecular dynamics simulations on bead-spring models of HA and ssDNA. The models are based on previous work that treated monovalent systems [44, 45], and consist of the same system used in previous publication [34] to treat trivalent ions. Matching the HA structure, beads are separated by 5.1 Å with a charge on every other bead. The HA stiffness is set by the spring constant $k_a = 15$ in the cosine angle potential, which corresponds to an intrinsic persistence length of 8 nm. The HA chain consists of 450 beads. The ssDNA-like chain is a flexible chain of 200 charged beads separated by 6.4 Å.

The diameter of all ions is set to 4 Å: an intermediate estimate of the interaction distance between a hydrated metal cation (*e.g.* Na^+) and a carboxyl anion, which are separated by just 2.92 Å for a direct interaction [46, 47]. This value represents a lower limit on the interaction distance for the larger hexamine cations, in the unlikely case of minimal ion hydration. In the previous publication [34], we show that a larger ion diameter (6 Å, the reported diameter of a hydrated CoHex cation [48]) does not qualitatively affect our results.

III. EXPERIMENTS

We use magnetic tweezers to measure force-extension curves of single PE chains of HA, ssDNA, and ssRNA in different salt conditions (example curves shown in Fig. 1A). The resulting elastic curves are analyzed to find the crossover force, f_c, that separates low-force swollen-chain elasticity, $L \sim f^\gamma$ with $\gamma \approx 2/3$ [49], from high-force elasticity in which the extension asymptotically approaches the contour length L_C as, typically, a worm-like chain [10, 12, 14]. It has been established that this crossover force is sensitive to the total (intrinsic plus electrostatic) persistence length, $f_c \sim k_B T/l_p$ [50]. Thus, f_c, extracted from force-extension curves reports on the salt dependence of the chain stiffness (see Fig. 1A). Others

have shown that the three PEs studied here undergo transitions out of the Pincus power law regime in the force range accessible to magnetic tweezers ($\sim 0.1 - 10$ pN) [10–12, 14].

There are two approaches to estimating f_c from force-extension curves. The first involves fitting the entire force-extension curve with a piecewise function that captures the expected low and high force elastic behavior [10]. Alternatively, for sets of force-extension curves on the same type of PE, we can multiplicatively shift curves at various salts onto a chosen reference curve, causing them to collapse (Fig. 1B, see also Appendix Fig. 11) [11]. The shift factors in force are proportional to f_c. This second method, termed "co-fitting," has a significant advantage: it does not require knowledge of a functional form describing chain elasticity. However, it gives f_c relative to the reference curve (unitless shift factor $\bar{f}$), rather than an absolute value, and so does not allow for comparison between different species of PEs without additional knowledge. Below, we use co-fitting onto reference curves to find the scaling of $\bar{f}$ with I for each PE, and then perform piecewise fits of the reference curves to find the reference curve crossover force f_c^{ref}. We then combine the parameters to define an inverse crossover force, $1/(\bar{f} f_c^{ref})$, proportional to l_p, at each I; this allows us to compare absolutely between the systems. Details of co-fitting and piecewise fitting of reference curves are described in Appendix A.

A. Experiments in 1:1 Salt

We analyze force-extension curves of ssDNA, ssRNA, and HA in varying concentrations of NaCl, and find our results are not consistent with OSF predictions. The HA data presented here are all newly measured (though some analysis of these data is included in our prior publication [34]). The ssDNA data are a combination of newly measured and re-analyzed data published in Ref. [10]. A subset of the ssRNA data were published in Ref. [12, 51] and the rest are as yet unpublished. All force-extension curves, rescaled by cofitting and color-coded by salt, are shown in the Appendix, Fig. 11 and 12.

From the elastic curves, we extract estimates of the chain stiffness, $l_p \sim 1/(\bar{f} f_c^{ref})$, for the different PEs. We find $1/(\bar{f} f_c^{ref})$ decays as a power law with I for the two ssNAs (Fig. 2A), while HA shows a plateau at high salt because its electrostatic stiffness has become small compared to its intrinsic stiffness ($l_p^0 \approx 5$ nm). After subtraction of the plateau (discussed in Appendix A), the adjusted inverse crossover force (proportional to l_p^{elec}) also decays as a

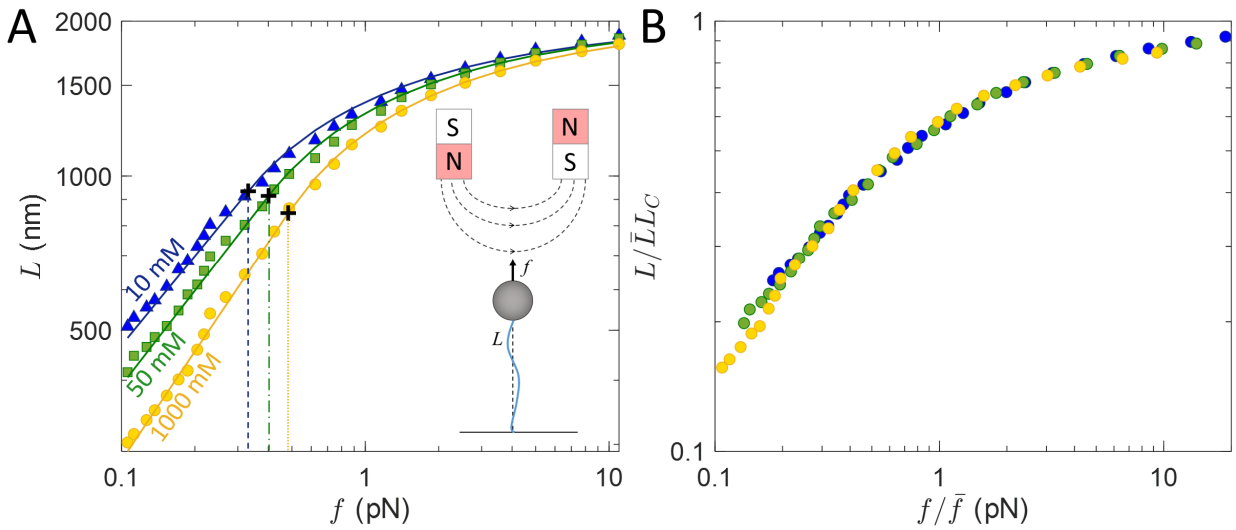

FIG. 1. A. Extension L versus applied force f for a single HA tether at 10 mM NaCl (blue triangles), 50 mM NaCl (green squares), and 1000 mM NaCl (yellow circles), all with 10 mM MOPS buffer, pH 7. Lines indicate best fits to Eq.A6, from which we extract estimates of the crossover force f_c, giving 0.33 ± 0.009 pN, 0.40 ± 0.009 pN, and 0.48 ± 0.006 pN for the 10, 50, and 1000 mM curves respectively. Inset shows a schematic of a tethered polymer stretched using magnetic tweezers. B. Force-extension curves from A, co-fit (multiplicatively shifted to achieve best overlap) onto a reference curve for HA in 50 mM salt. Fit unitless shift factors in force are $\bar{f} = 0.58$, 0.79, and 1.18.

power law for HA.

The inverse crossover force incorporates division by f_c^{ref} to eliminate dependence on the elasticity at the reference salt condition, which here is 50 mM. We note that at this choice of 50 mM, f_c^{ref} is very similar between the three PEs (0.50 ± 0.01, 0.64 ± 0.03, and 0.50 ± 0.01 pN for HA, ssDNA, and ssRNA respectively). This is likely because the stiffness of the less-charged HA has plateaued to near $l_p^0 \approx 5$ nm, while the more charged ssNAs still have significant electrostatic contributions, resulting in similar total stiffness values at 50 mM. As shown in Appendix A (Fig. 13), using a different reference salt concentration does not affect these results.

We use the crossover-force analysis to estimate the exponent, α, controlling the dependence of electrostatic stiffness on ionic strength, $l_p^{elec} \sim I^{-\alpha}$. In the data shown in Figure 2A, the slopes of the three data sets (corresponding to α) appear similar. Comparison of

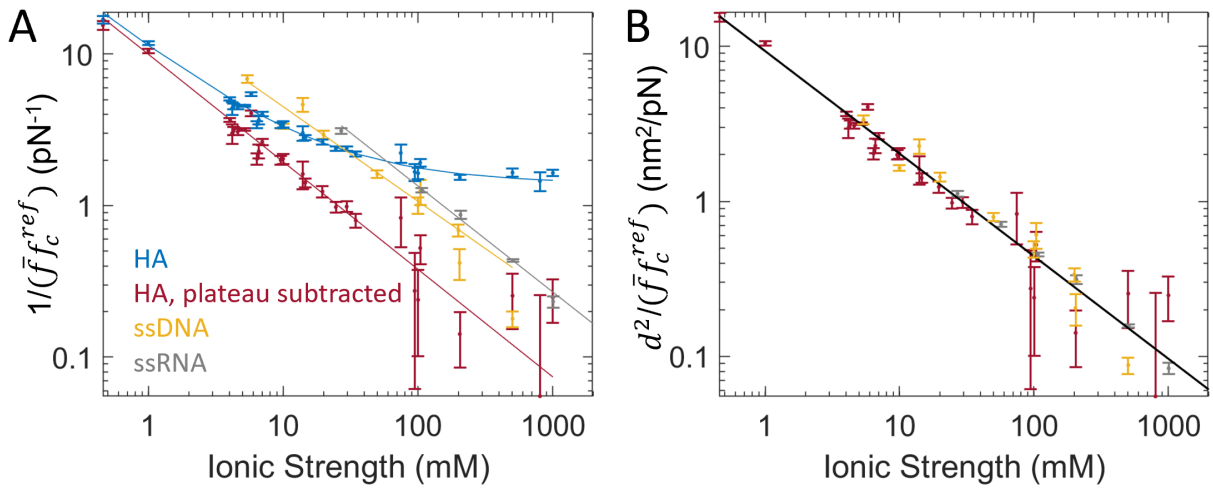

FIG. 2. A. Scaling with I of inverse crossover force $1/(\bar{f}f_c^{ref})$ for ssRNA (gray), ssDNA (yellow), and HA (blue/red). ssDNA and ssRNA data are fit with 1-parameter power laws with exponents $\alpha = 0.62 \pm 0.09$ and 0.70 ± 0.03 respectively (solid yellow and gray lines). Raw HA data (blue) are fit by Eq. A4 with $\alpha = 0.71$, $I_c = 16$ mM (dashed blue line). Plateau-subtracted HA data (red) are fit by a single parameter power law with exponent $\alpha = 0.71 \pm 0.02$ (solid red line). B. Multiplying the inverse crossover force by d^2 collapses the data from the three PEs onto a common curve (with $d^2 = 1$, 0.49, and 0.36 nm^2 for HA, ssDNA, and ssRNA). The combined dataset is fit by a power law with exponent $\alpha = 0.66 \pm 0.02$ (solid black line).

α values obtained from fitting (Table I) and their respective uncertainties (calculated from bootstrapping) shows no evidence of a statistically significant difference between the exponents. This observation is in contrast to prior work ([10, 11, 14], listed in Table I). It is possible that given the uncertainty in the data, we fail here to resolve small differences between the exponents. It is also possible that the sensitivity of co-fitting or piecewise fitting (e.g. to choices of initial guess or inclusion of outliers) could affect results, causing differences in different studies. Beyond the co-fitting, the value of α extracted from fits to the $1/(\bar{f}f_c^{ref})$ versus I data can itself be very sensitive to the inclusion or exclusion of points with small numbers of replicates, or to the choice of weighting scheme. These reasons likely explain the disagreement with past results on α for ssDNA. [10, 11]

We next consider whether differences in the charge spacing d are responsible for the absolute value differences shown in Figure 2. As discussed in Appendix A, we expect the

TABLE I. Estimates of scaling exponent α for HA, ssDNA, and ssRNA.

	HA	ssDNA	ssRNA
α from literature	0.65 ± 0.02 [14]	0.54 ± 0.03*† [10]	0.58 ± 0.09 [12]
		0.51 ± 0.04* [11]	
		0.47 ± 0.03*‡ [11]	
α measured	0.71 ± 0.02†	0.62 ± 0.09†	0.70 ± 0.03†

*Values obtained from piecewise fits (all others from co-fitting)

†Errors estimated from bootstrapping

‡Measured in KCl (all others in NaCl)

electrostatic persistence length (and thus $1/(\bar{f} f_c^{ref})$) to have the form

$$l_p^{elec} = Bd^{-2}I^{-\alpha}, \tag{2}$$

where B is a constant. The d^{-2} dependence arises because the screened Coulomb potential per unit charge is proportional to line charge density ($\sim 1/d$) [2, 4]. Given the lack of a statistically significant difference between α values fit here using the same algorithm, we assume that the same (or very similar) α describes the scaling of all three PEs. Thus, differences in the absolute values plotted in Fig. 2A should be attributable to differences in d^2. Fig. 2B confirms that multiplication by d^2 collapses the data onto a common curve, using $d = 1$ nm for HA, $d = 0.7$ nm for ssDNA, and $d = 0.6$ nm for ssRNA.

Fitting the combined collapsed data set yields $\alpha = 0.66 \pm 0.02$. This value is much lower than the OSF prediction of $\alpha = 1$. It is slightly larger than some previous estimates of α for ssNAs [10, 11] which were consistent with the BJ prediction of $\alpha = 0.5$ [15]. Our results are consistent with Netz-Orland modifications to OSF theory that predict $\alpha \approx 0.7$ by accounting for condensing monovalent ions [35], however, simulations have shown that this exponent may arise even without ion condensation for an HA-like chain [45]

We speculate that a simple alternative explanation may explain the observed scaling. DH theory predicts a screening length $\kappa_{DH}^{-1} = (8\pi l_B I)^{-1/2}$. However, the mean distance between ions in solution is $x_i \sim c_{ion}^{-1/3}$, where c_{ion} is the number density of ions in the bulk, equal to $2I$ in 1:1 salt. Although the exact pre-factor for calculation of x_i is not clear, scaling dictates that at high enough salt, x_i exceeds κ_{DH}^{-1}, meaning DH theory predicts the electric field is

TABLE II. Comparison of Debye screening length κ_{DH}^{-1} and mean inter-ion spacing $x_i = (2I)^{-1/3}$. Note: Other geometric choices of prefactor for calculation of x_i could be reasonable.

I (mM)	κ_{DH}^{-1} (nm)	x_i (nm)
1	9.6	9.4
10	3.0	4.4
100	0.96	2.0
1000	0.30	0.94

screened over a distance in which there are on average no ions (Table II). As an alternative to this seemingly unphysical picture, we posit the Debye screening length can be replaced by the mean inter-ion spacing x_i. Replacing κ_{DH}^{-1} in the traditional OSF expression (Eq. 1) with x_i results in an l_p^{elec} which scales with $c_{ion}^{-2/3}$, consistent with the experimental results shown here (since $c \sim I$ in 1:1 salt).

B. Experiments in Z:1 Salt

When multivalent salt is present in solution, we expect a complex interplay between strong ion-PE interactions and weaker screening effects, motivating the need for experiments on single PE chains in carefully controlled salt conditions. We study the case of a small, constant concentration of multivalent salt alongside varying amounts of added 1:1 salt. Our experimental systems are (1) HA with 0.1 mM 3:1 salt (either Cobalt (III) Hexamine Chloride (CoHex) or Ruthenium (III) Hexamine Chloride (RuHex), data reported in our previous publication [34]), and (2) ssDNA with 1 mM 2:1 salt ($CaCl_2$), to which we add NaCl to increase the ionic strength. Previously we showed no difference between HA elasticity in CoHex versus RuHex [34], and the data presented here combine measurements on both. We co-fit force-extension curves measured in the presence of multivalent salt onto the same reference curves used for the monovalent-only data set, taken at $I_{ref} = 54$ mM. Co-fit multivalent salt data are shown in Appendix A, Fig. 12.

We find a large regime in which both systems show no dependence on the NaCl. Fig. 3 shows the I-dependence of the multivalent-containing curves alongside the 1:1-salt data. At

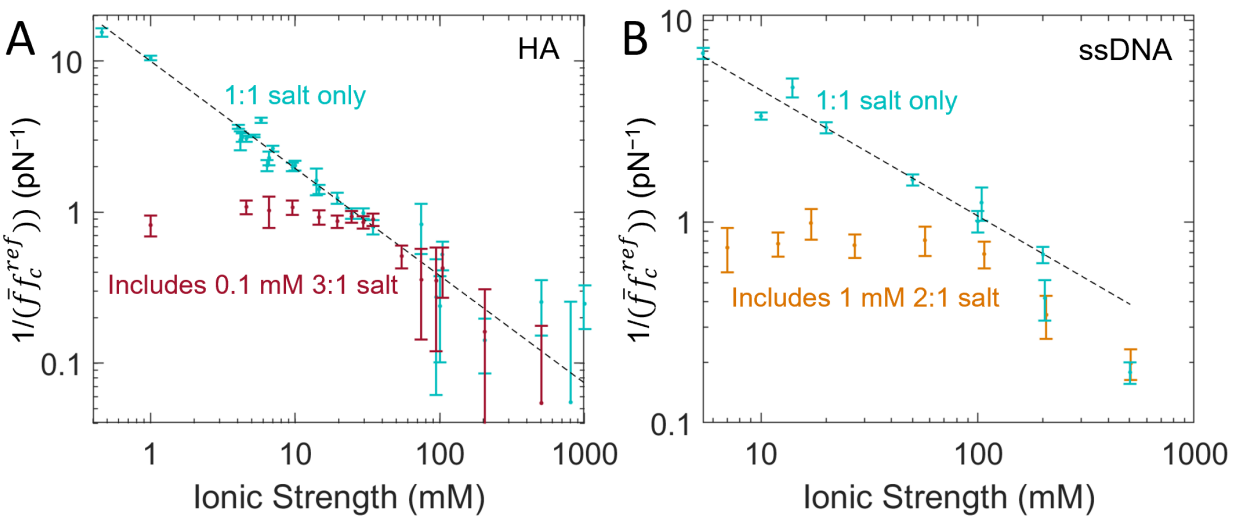

FIG. 3. Inverse crossover force $1/(\bar{f}f_c^{ref})$ as 1:1 salt is added to increase I, with and without a small constant amount of multivalent salt. A. HA, with and without 0.1 mM 3:1 salt. Blue: 1:1 salt only. Red: combined trivalent data set. Blue points and associated fit are reproduced from Fig. 2. The plateau value has been subtracted from HA data. B. ssDNA with and without 1 mM 2:1 salt. Blue: 1:1 salt only. Orange: $CaCl_2$. Blue points and associated fit are reproduced from Fig. 2.

low and moderate salt, the values of inverse crossover force $1/(\bar{f}f_c^{ref})$, which are proportional to l_p^{elec}, are much smaller than in 1:1 salt of equal I. However, over a large range, the values do not change as NaCl is added. This plateau persists until the multivalent-affected data curve meets the 1:1-only curve. Beyond that point they are indistinguishable and $1/(\bar{f}f_c^{ref})$ decreases with I as expected. The I-insensitive regime persists until about 30 mM for the HA/trivalent system and up to about 100 mM for the ssDNA/divalent system. To our knowledge, this regime of ionic strength insensitivity has not been predicted theoretically.

IV. SIMULATION RESULTS

Simulations can provide understanding of the microscopic origins of ionic strength insensitivity in the presence of multivalent ions. Coarse-grained molecular dynamics simulations were previously shown to give a good approximation of the real elastic behavior of a charged chain, including in the presence of trivalent ions [34]. Simulations of HA-like and ssNA-like

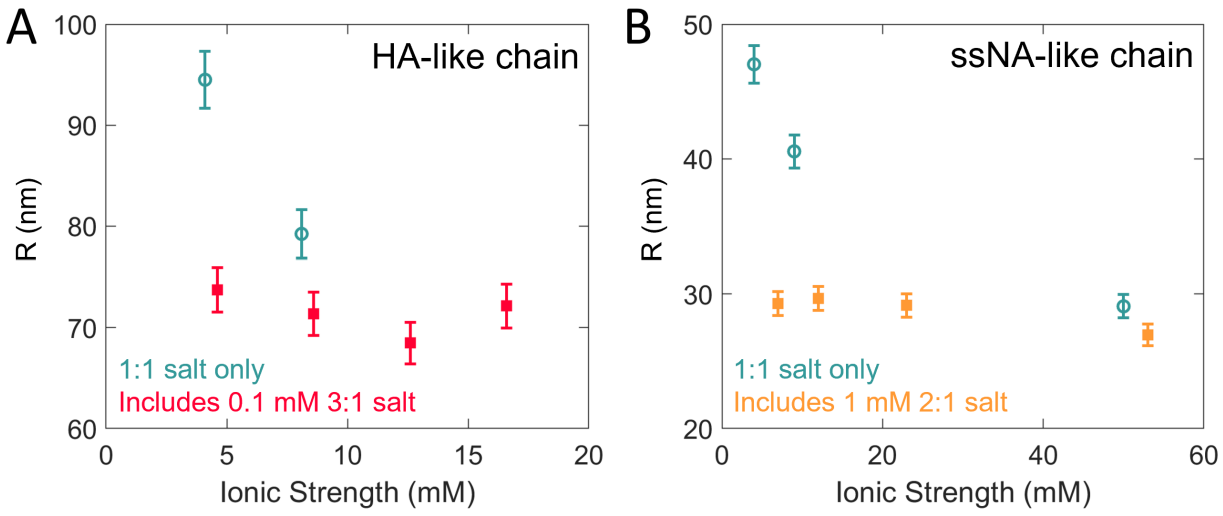

FIG. 4. Simulated chain average end-to-end extension R under no applied force, as a function of ionic strength I. A. HA-like chain with (red squares) and without (blue circles) 0.1 mM 3:1 salt. B. ssNA-like chain with (orange squares) and without (blue circles) 1 mM 2:1 salt. Error bars show standard error of the mean, approximately ±3% and ±6% for the HA and ssNA systems respectively.

PEs with multivalent ions reproduce the same regime of extensional salt-independence observed at low forces in experiments (Fig. 4). Based on the similarity between simulation and experimental behavior, and in agreement with previous work [45], we conclude that the simulations provide a good approximation, and examine microscopic details in the simulated system to glean information about how the ions control PE elasticity.

Simulations show no evidence of the chain wrapping or bending around ions. As discussed previously [34], examination of the structure factor for the simulated HA-like chain rules out the possibility of distinct local structures (on scales $< l_p^0$) induced by binding multivalent ions. This indicates instead that the effect is caused by long-range, non-specific electrostatic interactions. It does not rule out the existence of specific multivalent ion interactions (which others have observed, *e.g.,* for HA and calcium [52]), but shows that they are not necessary for the effect we observe here.

As we do not observe major contributions from ion-induced short length-scale structure changes, we next examine the local ion environment, including strongly interacting multivalent cations and weakly associated monovalent cations. We define the local environment by examining the radial charge profile near the PE. Figure 5 shows the net charge enclosed as a

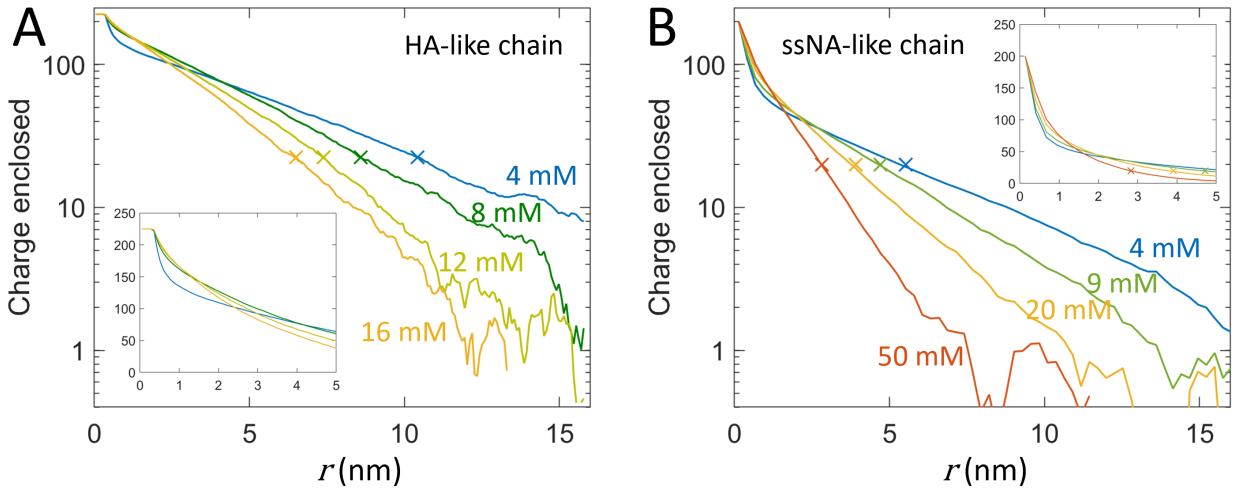

FIG. 5. Charge enclosed in a cylinder centered at the chain, from simulation, as a function of distance r from the chain. A. HA-like chain (225 negative charges) with 0.1 mM 3:1 salt and 4–16 mM 1:1 salt. B. ssNA-like chain (200 negative charges) with 1 mM 2:1 salt and 4–50 mM 1:1 salt. Insets are zoomed in on region near the chain and linearly scaled to show the precipitous decrease in total enclosed charge due to a layer of closely associated multivalent counterions.

function of distance r from the chain. At short distances (and especially when salt is low), a steep region is visible, corresponding to a layer of closely associated multivalent counterions. Beyond that initial region, the charge decreases with a slope that depends on total salt. We define the local region as a cylinder approximating the distance to reach charge neutrality, i.e. when the chain charges are all compensated by the excess cations attracted (strongly or weakly) to the chain. In practice, the data get very noisy as net charge approaches zero, so we define our charge neutrality radius R_{cyl}^{neut} as the distance to achieve 90% charge neutralization in the simulation, indicated by x's in Fig. 5.

We then count the ions within the local cylinder. These ion numbers are listed in Tables III and IV. It is worth noting that nearly all the multivalent cations are situated extremely close to the chain, while the monovalent ones are more dispersed throughout the cylinder. This is consistent with condensation, as expected due to the strong electrostatic attraction between the multivalent cations and the PE. It is further expected that increasing 1:1 salt should progressively screen these condensation interactions. Tables III and IV confirm that as 1:1 salt is added, fewer multivalent cations remain near the chain. However, as shown in Fig. 3 and 4, this loss of condensed ions does not lead to a change in elasticity, presumably

1:1 salt (mM)	3:1 salt (mM)	R_{cyl}^{neut} (nm)	R_{cyl}^{neut}/x_i	$R_{cyl}^{neut}/\kappa_{DH}^{-1}$	# ions within R_{cyl}^{neut}		
					+3	**+1**	**-1**
4	0.1	10.4	1.79	2.32	32	251	144
8	0.1	8.6	1.84	2.62	15	359	200
12	0.1	7.4	1.81	2.73	10	400	228
16	0.1	6.5	1.75	2.75	8	410	231

TABLE III. Ion environment near simulated HA-like chain with 0.1 mM 3:1 salt and 4–16 mM 1:1 salt. At each salt condition, radius R_{cyl}^{neut} of the 90% charge-neutral cylinder is proportional to x_i, the mean bulk ion spacing. The final three columns list number of ions within R_{cyl}^{neut}.

1:1 salt (mM)	2:1 salt (mM)	R_{cyl}^{neut} (nm)	R_{cyl}^{neut}/x_i	$R_{cyl}^{neut}/\kappa_{DH}^{-1}$	# ions within R_{cyl}^{neut}		
					+2	**+1**	**-1**
4	1	5.52	1.04	1.19	74	46	14
9	1	4.71	1.10	1.50	61	72	22
20	1	3.91	1.16	1.84	43	129	35
50	1	2.83	1.12	2.08	21	185	47

TABLE IV. Ion environment near simulated ssNA-like chain with 1 mM 2:1 salt and 4–50 mM 1:1 salt. At each salt condition, radius R_{cyl}^{neut} of the 90% charge-neutral cylinder is proportional to x_i, the mean bulk ion spacing. The final three columns list number of ions within R_{cyl}^{neut}.

due to the compensating increase in nearby monovalent ions.

Tables III and IV also list cylinder radius R_{cyl}^{neut}, which depends on salt. Interestingly, the salt-dependence of R_{cyl}^{neut} collapses when it is rescaled by $x_i = c_{ion}^{-1/3}$, the mean bulk ion spacing, and *not* by the bulk Debye length. This supports the idea that x_i, rather than κ_{DH}^{-1}, is the relevant length scale. As discussed previously, this idea is consistent with the $l_p^{elec} \sim I^{-0.66\pm0.02}$ scaling observed for the PEs in 1:1 salt. The factor of proportionality (Tables III, IV, Column 4) is of order 1, and differs slightly between the HA-like and ssDNA-like chains (1.8 versus 1.1), likely due to differences in flexibility.

In the following section, we incorporate this new information about the size of the local neutralizing ion environment to build a model of how ion exchange within a local jacket

leads to an I-insensitive PE stiffness.

V. THEORETICAL MODEL

Our theoretical model aims to predict the condensation-renormalized PE charge spacing d_{eff} in salt mixtures, reflecting the multivalent-monovalent ion exchange observed in our simulations (Tables III and IV). Based on the collapse of $1/(\bar{f}f_c^{ref})$ versus I data for HA and ssNAs (Fig. 2B), we expect that when multiplied by the correct d_{eff}^2, the multivalent-induced plateau shown in Fig. 3 will collapse back onto the $I^{-0.66}$ curve observed in 1:1-only salt (for which we expect condensation effects are minimal).

To predict the number of condensed ions (and thus d_{eff}) as a function of added 1:1 salt, we introduce a three-state model (Figure 6). An ion may be (1) condensed directly on the chain, (2) uncondensed but constrained within a local, charge neutral volume, termed here an "ion jacket, or (3) free in the bulk solution. We first invoke Donnan equilibrium between regions (2) and (3) to calculate the concentrations of each type of ion within the ion jacket, and then use those concentrations to define a local screening length that controls ion condensation within a two-state model. The subsequent two-state approach (i.e. between regions (1) and (2)) assumes a condensed ion interacts with the chain via an unscreened site binding term, the Born energy $-Zl_B/a$ [53], where a is the distance of closest approach, taken to be 4 Å, in addition to a screened interaction with the rest of the chain, modeled as a uniformly charged cylinder. As described in detail below, we also include a mixing entropy term for site-bound ions, and we then equate the bound ion chemical potential with that of an uncondensed ion within the local jacket. Our model predicts an ion exchange within the condensed and jacket regions consistent with our simulations and experimental results.

The approach we take here is inspired by existing theories, including Manning's two-variable theory [21] and the similar two-state model of Burak, Ariel, and Andelman (BAA) [22]. These models describe an exchange between bulk and condensed ions, predicting that as 1:1 salt is added, the electrostatic interaction driving condensation will be screened. However, these models assume that a condensed ion interacts with a uniformly charged cylindrical PE via a screened electrostatic potential. In some cases this may lead to an underestimate of condensation due to the large energy associated with a counterion condensing directly on a chain charge. We thus include a site binding (Born) term; however, this addition alone

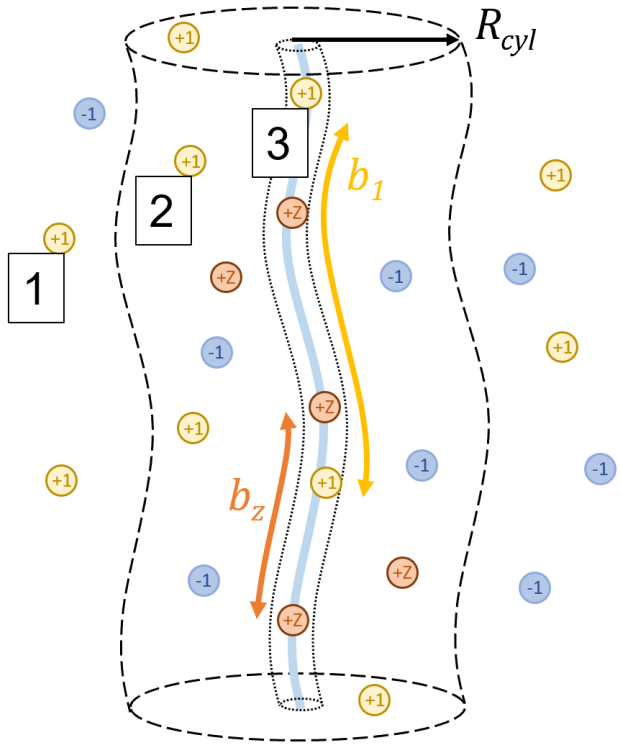

FIG. 6. Illustration of three-state model for ions interacting with the PE . An ion may be (1) free in the bulk solution, (2) free to move within a charge-neutral local jacket whose composition is dictated by Donnan equilibrium, or (3) condensed on the charged chain.

leads to a model that overestimates condensation at low ionic strength. To resolve this, we incorporate an intermediate state between condensed and free," corresponding to those ions constrained within the local jacket. This addition is supported by our simulations, which show ions are enhanced in the region near the charged chain, necessitating definition of a *local* screening length that governs the interaction of condensed ions with the nearby cylindrical PE. This picture is consistent with the cylindrical cell model of macroions in salt-containing solutions, discussed in Ref. [25].

A. Donnan equilibrium

Based on our simulations, we define the ion jacket as the local charge neutral environment: a cylinder of radius $R_{cyl} = R_{cyl}^{neut} = ux_i$, where $x_i = c_{ion}^{-1/3}$ is the mean distance between ions in the bulk solution, and u is a constant of order 1, taken from simulations as $u = 1.8$ for

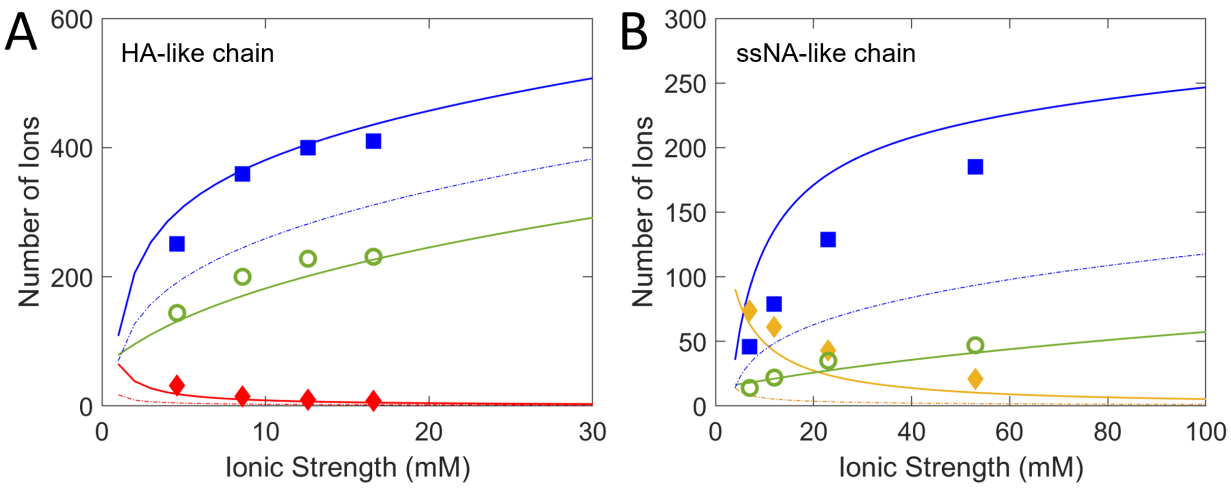

FIG. 7. Number of ions within a cylinder of radius $R_{cyl} = ux_i$. Symbols show ion numbers from simulation, solid curves show Donnan model predictions. Blue: monovalent cations, green: monovalent anions, red/orange: tri-/divalent cations. Dot-dashed lines show the number of expected cations if all ions were uniformly distributed. A. HA-like chain + 0.1 mM 3:1 salt. B. ssNA-like chain + 1 mM 2:1 salt.

the HA system, and $u = 1.1$ for the ssDNA system (Tables III and IV). Within the jacket volume $V = L_c \pi R_{cyl}^2$, we use a Donnan equilibrium approach [54], treating the cylinder as a membrane permeable to free ions but impermeable to the PE charges. This approach, described in detail in Appendix B, dictates how each ion species will be distributed on either side of the cylinder, subject to both compartments maintaining charge neutrality.

The ion numbers calculated from this model are in good agreement with those from simulation, as shown in Fig. 7. With the total number of ions in the jacket predicted by Donnan equilibrium, we then use a two-state condensation model, similar to Ref. [34]. Instead of the bulk ion concentrations, we will use the concentrations inside the Donnan volume.

B. Condensation equations

In order to solve for the number of condensed ions, we equate the chemical potential for a condensed and free ion within the Donnan cylinder. Inside the cylinder of volume $V = L_c \pi R_{cyl}^2$, there are $n_{Z,in}$ Z-valent cations (including both free and condensed), $n_{+,in}$

monovalent cations (free and condensed), and $n_{-,in}$ monovalent anions. d_Z (d_1) is the spacing between Z(1)-valent ions that are condensed onto the chain, giving a number of condensed ions equal to L_c/d_Z. The ideal gas chemical potential for a "free" Z-valent cation in the cylinder of volume V is given by:

$$\mu_Z^{free} = \ln \frac{\left(n_{Z,in} - \frac{L_c}{d_Z}\right) a^3}{V} \tag{3}$$

where a is the ion size. We assume that a free ion in the charge-neutral cylinder sees on average no electrostatic potential. We then write the chemical potential for a condensed Z-valent cation:

$$\mu_Z^c = -\frac{Zl_B}{a} - \frac{2Zl_B}{d}\left[-\ln\left(1-e^{-\kappa d}\right)\right] + \frac{2Zl_B}{d_1}\left[-\ln\left(1-e^{-\frac{\kappa d_1}{2}}\right)\right] + \frac{Z^2 l_B}{d_Z}\left[-\ln\left(1-e^{-\kappa d_Z}\right)\right] - \ln\left(d_Z\left(\frac{1}{d}-\frac{1}{d_1}\right)\right) \tag{4}$$

where κ is defined using $c_{Z,in}$, $c_{+,in}$, and $c_{-,in}$ predicted by the Donnan model, and not the bulk ion concentrations. The first term is the Born energy [53], the second term gives the screened attractive interaction with the negatively charged chain, the third and fourth terms give the screened repulsive interactions with other condensed cations (monovalent and Z-valent, respectively), and the fifth term accounts for mixing entropy from possible rearrangements on available sites. The condensation of monovalent cations is governed by equivalent expressions, though the extent of monovalent condensation is small, even for [1:1] $\sim$ 100 mM. We solve the system of two equations for the two unknown condensed ion spacings d_Z and d_1, which in turn yield $d_{eff} = \frac{L_c}{N_0 - ZL_C/d_Z - L_C/d_1}$, where N_0 is the number of PE charges (see Fig. 8).

We next evaluate whether the renormalized charge spacing predicted by our model can explain the insensitivity of l_p^{elec} to I when multivalent salt is present. For the monovalent-only measurements (for which little to no condensation is expected), we find that multiplication by the PE structural charge spacing squared collapses the data onto a common curve that decays as $I^{-0.66}$ (Fig. 2). If we replace d with the predicted d_{eff}, we indeed find that the multivalent containing systems display a similar salt scaling to the monovalent-only ones (Fig. 9). The collapse of the rescaled data shows our model is sufficient to explain the experimental results.

The salt dependent effective charge spacing from our model accounts for the unexpected regime of salt-insensitivity. In Fig. 10, we compare alternative means of calculating the

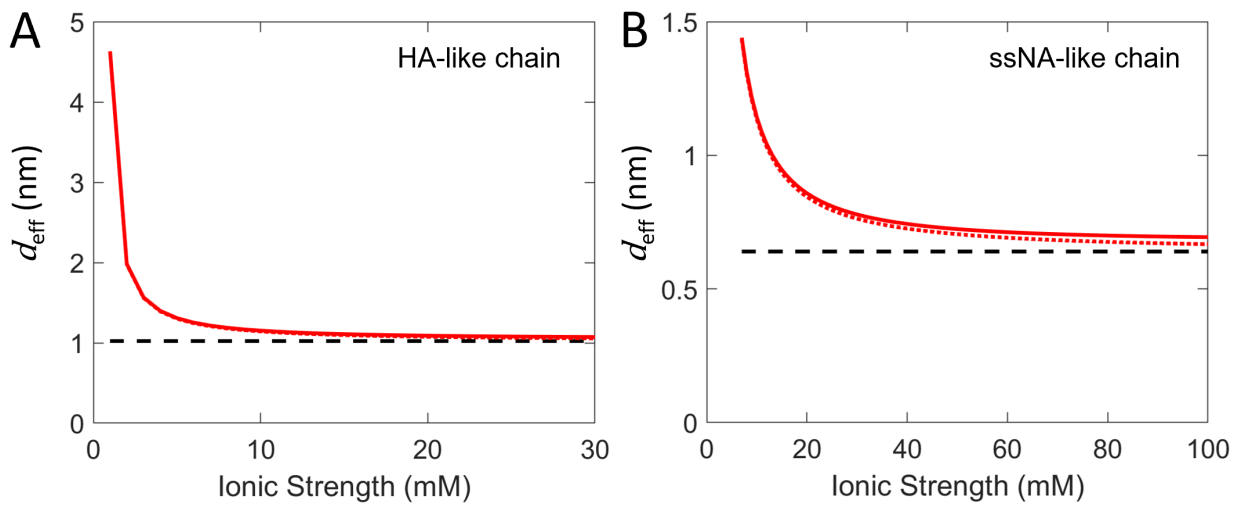

FIG. 8. Renormalized chain charge spacing d_{eff} predicted from the Donnan/condensation three-state model. A. HA + 0.1 mM 3:1 salt. B. ssDNA + 1 mM 2:1 salt. Thin dotted red line shows d_{eff} neglecting monovalent condensation. Dashed black line shows the structural charge spacing d.

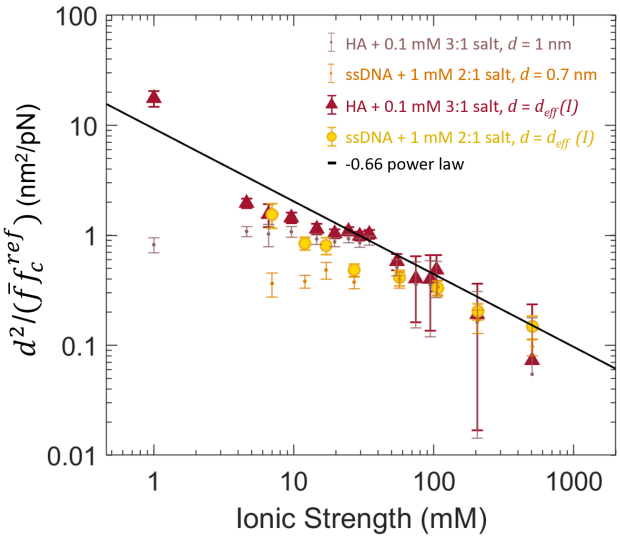

FIG. 9. $I^{-0.66}$ scaling of inverse crossover force in monovalent salt (black line), reproduced from Figure 2B, alongside data on HA + 0.1 mM 3:1 salt and ssDNA + 1 mM 2:1 salt, which show plateaus when multiplied by the structural charge spacing d^2 (HA: purple points, ssDNA: yellow points), but collapse nearly onto the expected curve when d_{eff}^2 is used instead (HA: dark red circles, ssDNA: yellow circles).

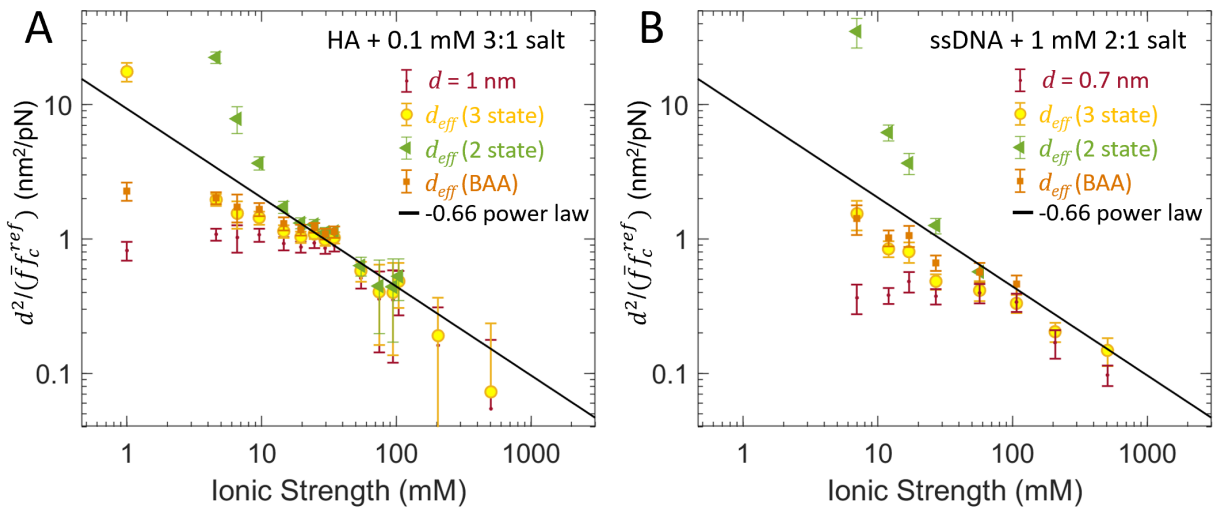

FIG. 10. Comparison of condensation models used to calculate I-dependent d_{eff} to replace structural charge spacing d in the normalization. Red points are multiplied by d^2. Yellow circles use d_{eff} calculated from our three-state model. Green triangles use d_{eff} calculated from a two-state model with no locally enhanced screening. Orange squares show result of the BAA model [22]. Black line shows $\alpha = 0.66$ power law fit to all monovalent-only data. A. HA + 0.1 mM 3:1 salt. B. ssDNA + 1 mM 2:1 salt.

renormalized charge spacing. The BAA model [22] produces very similar d_{eff} values to our model over most of the salt range studied; however, the HA data shows that it underestimates condensation at very low salt (orange squares in Fig. 10A). A two-state model that includes a Born energy term but assumes screening dictated by bulk κ_{DH} dramatically overestimates condensation at low salt (green triangles, Fig. 10). We conclude that our three-state model, which accounts for some inhomogeneity in the uncondensed ion atmosphere in addition to the discrete nature of chain charges, is most successful at describing condensation in these salt regimes.

VI. CONCLUSIONS

We have measured the behavior of several charged biopolymers in varying concentrations of 1:1 salt and in multivalent salt mixtures. We first found the electrostatic stiffness, when properly adjusted for the charge spacing d, demonstrated a universal scaling with ionic strength for HA, ssDNA, and sRNA in 1:1 salt (Fig. 2). This universal behavior is somewhat

remarkable, given the differences between the chains: the intrinsic stiffness of HA ($l_p^0 \approx 5$ nm [14, 36]) far exceeds that of the nucleic acids ($l_p^0 < 1$ nm[37]). Further, the chemical identity of the charges differs between HA and the ssNAs (carboxyls versus phosphates), and the bases of the ssNAs constitute side chains that are not present in HA.

The universal value, for all three chains, of the measured scaling exponent of electrostatic stiffness with salt, $l_p^{elec} \sim I^{-\alpha}$ with $\alpha = 0.66 \pm 0.02$, disagrees with standard theoretical predictions. The scaling is consistent with our modified OSF suggestion, in which we posit the screening length is set by the inter-ion spacing $x_i \sim c^{-1/3}$ rather than by κ_{DH}^{-1}. This approach is attractive as it would also explain why, in the simulations, the charge neutrality distance $R_{cyl}^{neut} \sim x_i$. However, this explanation is not a full theory, so more work is needed to explore it.

Alternatively, the exponent could be explained by the theory of Netz and Orland [35], in which OSF scaling with ionic strength is modulated by salt-dependent condensation. This theory was recently invoked to explain the scaling of l_p with salt for dsDNA [8]. However, the Netz-Orland viewpoint does not explain the behavior of R_{cyl}^{neut}. Golestanian et al. [28] also propose a modified OSF formula whose prediction at low salt is consistent with our scaling behavior for certain parameter choices. However, that theory focuses on stiff PEs, and the prediction diverges from power-law-like behavior at relatively modest salt; in contrast, our data is on flexible PEs, and the power-law persists to high salt. Thus, while intriguing, the Golestanian prediction seems unlikely to be relevant to the present results.

If small amounts of multivalent salt are present, our experiments show that altering I by addition of monovalent salt has no effect on PE behavior over a large range of I. We demonstrated this effect on HA with 0.1 mM 3:1 salt and on ssDNA with 1 mM 2:1 salt. Coarse-grained molecular dynamics simulations reproduced the effect and provided microscopic information about the structure of the ion environment near the chain, notably demonstrating that the diameter of the local charge-neutral cylinder (i.e. the ion jacket region) scales with x_i rather than κ_{DH}^{-1}. We incorporate this scaling relation, along with a numerical prefactor, also from simulation, into a new model, combining Donnan equilibrium between the bulk and the jacket region with a model for condensation. This three-state model reproduces the ion-exchange phenomena seen in simulation, in which increasing bulk monovalent salt concentration leads to exchange of multivalent for monovalent salt within the jacket region, thus weakening condensation (i.e. decrease of d_{eff}, Fig. 8) in a manner that

counteracts the effects of increasing ionic strength. Apart from matching the simulation, the success of this model is demonstrated by the collapse of experimental data from two distinct PEs when rescaled by the calculated value of d_{eff}.

Our results have implications on the behavior of the studied biopolymers in applied or biological situations. Other work [55] has shown that trivalent cations can, under some circumstances, crosslink HA. Understanding the I-dependence of the electrostatic ion-chain interactions may help in developing stable (and even tunable) HA materials. Most biological environments have $I > 100$ mM; this is above the salt-insensitive regime for HA with 0.1 mM trivalent ions, and this may have implications on the stability of ionic crosslinks. While free trivalent cations are not commonly present in biological solutions, divalent cations are usually found at concentrations $\sim$1 mM, alongside monovalent ions at concentrations of 100–200 mM [56–59]. Based on the experiments conducted here, this physiologically relevant condition appears to be roughly the point at which ssDNA transitions from I-insensitive to I-responsive. As such, the I-insensitive regime may have relevance for the conformation of ssNAs inside biological cells.

Appendix A: Details of co-fitting

1. Co-fitting to find salt-dependence of crossover force

Co-fitting a set of force-extension curves in different salt conditions enables us to estimate the scaling of the crossover force with ionic strength. We first select a reference salt condition, I_{ref}, and average all force-extension curves taken at I_{ref} to create a smooth reference curve. The reference curves are shown in Figure 11, and are taken at 50 mM NaCl with 10 mM MOPS, pH 7, for HA and ssDNA, and 10 mM Tris HCl, pH 7.5, for ssRNA. The number of 50 mM curves averaged to create the reference curve is 13 for HA, 8 for ssDNA, 4 for ssRNA. For all force-extension curves measured at other values of I, we shift by constant factors in force and length ($\bar{f}$ and $\bar{L}$) to achieve the best overlap with the reference curve. This is accomplished by interpolating both the reference curve and the curve to co-fit at log-spaced intervals and minimizing the sum of squared errors in length per overlapping point. Fig. 11 shows force-extension curves at various values of I co-fit onto the 50 mM reference curves.

Force-extension curves on HA and ssDNA measured with multivalent salt were co-fit onto

the same reference curves as the monovalent salt data; the results of co-fitting are shown in Fig. 12.

There are some limitations to the co-fitting procedure. It implicitly assumes the elastic behavior is dictated by just two length scales and does not account for other aspects of the chain structure that may be altered by salt (e.g. the excluded volume parameter approaching zero). Previous work has shown some residual salt-dependence in low-force elasticity after co-fitting [14]. Additionally, co-fitting is only effective for force-extension curves that sample regimes on either side of the crossover; if it does not (e.g. a flexible chain at very high salt will not sample the high-force regime), then there will be no minimum in the cost function, and the output will be determined by the initial guess. This tends to cause difficulties in co-fitting at extreme salt conditions. For this reason, we conduct all our measurements at or below 1 M salt.

The crossover force of a curve is related to the unitless shift factor $\bar{f}$ according to $f_c = \bar{f} f_c^{ref}$. The reference curve crossover force is $f_c^{ref} = \frac{C_1}{l_p^{ref}}$, where C_1 is a constant with units of energy and does not depend on the PE system, and l_p^{ref} is the total persistence length of the PE at $I = I_{ref}$. Thus for any curve shifted onto the reference curve,

$$\frac{1}{\bar{f}} = \frac{l_p}{l_p^{ref}} = \frac{l_p f_c^{ref}}{C_1} = \frac{f_c^{ref}}{C_1}(l_p^0 + l_p^{elec}). \tag{A1}$$

We take the form of the electrostatic persistence length to be

$$l_p^{elec} = B d^{-\beta} I^{-\alpha}, \tag{A2}$$

where B is a constant that does not depend on the PE, d is the PE charge spacing, and $\beta = 2$ following Ref. [2, 4], because the screened Coulomb potential *per unit charge* is proportional to line charge density. The form of Eq. A2 is supported by data on ssNAs (for which $l_p \approx l_p^{elec}$) showing $1/\bar{f}$ decays as a power law with I (Fig. 2). We plug l_p^{elec} from Eq. A2 into Eq. A1, giving:

$$\frac{1}{\bar{f}} - \frac{f_c^{ref}}{C_1} l_p^0 = C_2 f_c^{ref} d^{-\beta} I^{-\alpha} \tag{A3}$$

where constant $C_2 = B/C_1$ does not depend on the PE system.

From Eq. A3, it is clear that the persistence length of a PE with a significant intrinsic stiffness will behave as a $-\alpha$ power law when salt is low, and plateau to a constant when salt

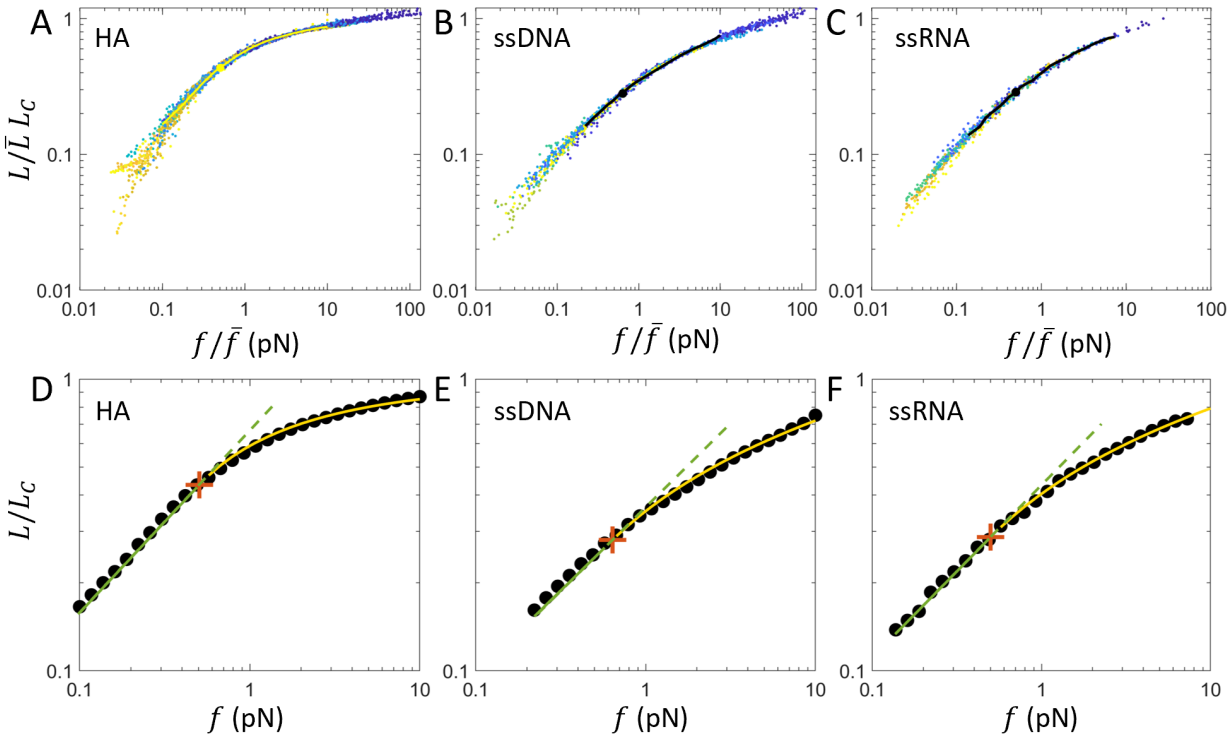

FIG. 11. Cofitting onto reference curves. A.–C. n force-extension curves at various concentrations of 1:1 salt are co-fit onto reference curves on the same PE at 50 mM NaCl. Salt ranges from 1 mM to 1000 mM, with low salt data in blue and high salt data in yellow. A. HA, $n = 274$. B. ssDNA, $n = 59$. C. ssRNA, $n = 33$. D.–F. Reference curves fit by piecewise functions (Eq. A6 and A7). Crossover at f_c^{ref} is indicated by an orange cross. Low force power law of exponent γ, green, is extended to $f > f_c^{ref}$ with a dashed line to show deviation above the crossover. Yellow curves show high force fits. D. HA, $\gamma = 0.62$, $f_c^{ref} = 0.50 \pm 0.01$ pN. E. ssDNA, $\gamma = 0.57$, $f_c^{ref} = 0.64 \pm 0.03$ pN. F. ssRNA, $\gamma = 0.60$, $f_c^{ref} = 0.50 \pm 0.01$ pN. $\bar{f}$ and $\bar{L}$ denote shift factors in force and length, L_c denotes chain contour length, estimated from WLC fit.

is high. Let I_c denote the ionic strength above which the stiffness plateaus and I_{ref} denote the reference salt condition. The behavior is described by the following expression [14]:

$$\frac{1}{\bar{f}} = \frac{1}{1 + \left(\frac{I_c}{I_{ref}}\right)^{\alpha}} + \frac{I_c^{\alpha} I^{-\alpha}}{1 + \left(\frac{I_c}{I_{ref}}\right)^{\alpha}}. \tag{A4}$$

HA has significant intrinsic stiffness ($l_p^0 \approx 5$ nm) and plots of $1/\bar{f}$ clearly show the expected plateau (Figure 2A). We fit the HA data with Eq. A4 and extract estimates of I_c and α, listed in Figure 2 caption. These parameters allow us to calculate and subtract off the

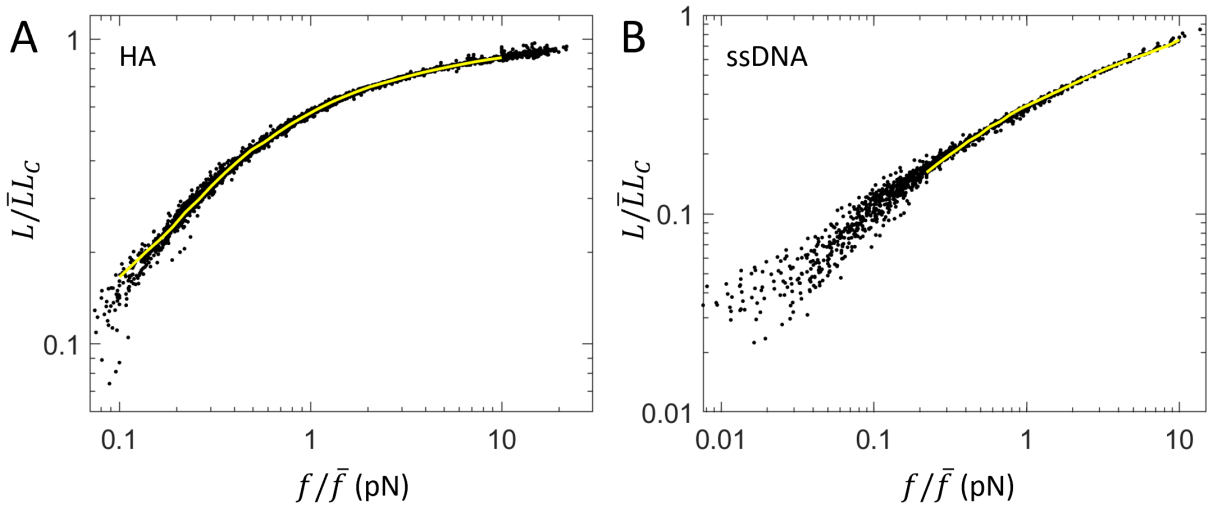

FIG. 12. Cofitting n force-extension curves with multivalent salt (black) onto reference curves taken in 54 mM monovalent salt (yellow). A. HA + 0.1 mM 3:1 salt, n=170. B. ssDNA + 1 mM 2:1 salt, n=63. $\bar{f}$ and $\bar{L}$ denote shift factors in force and length.

plateau value to plot a quantity proportional to the electrostatic persistence length (which decays as $I^{-\alpha}$), and redo the fit as a single-parameter power law. For the ssNAs, the intrinsic stiffness is very small, and the $1/\bar{f}$ data show no sign of a plateau. In both cases, we extract α as a fit parameter. Values of α are shown in Table I and Figure 2.

2. Piecewise fitting to find crossover force of reference curve

The above method is a powerful way to analyze scaling with salt, but, because everything is defined relative to a reference curve, it does not give the absolute value of l_p^{elec} for the different PEs. To compare absolutely between the PEs, we must account for the stiffness at I_{ref}, which is in general different for the different PEs. Eq. A3 and A4 each give an expression for $1/\bar{f}$; we can equate the I-dependent terms in each, giving:

$$\frac{1}{\bar{f}} - \frac{1}{1+\left(\frac{I_c}{I_{ref}}\right)^{\alpha}} = C_2 f_c^{ref} d^{-\beta} I^{-\alpha} \tag{A5}$$

where the constant term subtracted on the left-hand side is assumed to be negligible for the ssNAs. C_2 is a constant independent of PE identity, but to compare between PEs, we must first account for the different values of f_c^{ref}, which depends on choice of I_{ref} in addition to

PE species. Once f_c^{ref} has been divided out, any remaining differences between PEs must be ascribed either to differences in the charge spacing d, or in the scaling exponents.

We estimate the reference curve crossover force f_c^{ref} by fitting a piecewise function with the following characteristics: below f_c^{ref}, it behaves as a power law with exponent γ ($\gamma = 2/3$ is expected [49]), and above f_c^{ref}, HA behaves as a wormlike chain, while ssNA behavior is well-approximated by log scaling [33]. Following Refs [10, 11], we define continuous functions with continuous first derivatives with the expected low force power law and high force behavior:

$$L = L_c^{ref}\left(\frac{f}{f_c^{ref}}\right)^{\gamma} H(f_c^{ref} - f) + L_c^{ref}\left[-2\gamma\left(\frac{f_c^{ref}}{f}\right)^{1/2} + 2\gamma + 1\right] H(f - f_c^{ref}) \tag{A6}$$

$$L = L_c^{ref}\left(\frac{f}{f_c^{ref}}\right)^{\gamma} H(f_c^{ref} - f) + L_c^{ref}\left[\gamma \ln\left(\frac{f}{f_c^{ref}}\right) + 1\right] H(f - f_c^{ref}) \tag{A7}$$

where $H(x)$ is the Heaviside step function. Eq. A6 is used to fit the HA reference curve and Eq. A7 is used to fit the ssNA reference curves. In a first pass, we assume $\gamma = 2/3$, however, in practice we find that γ is often slightly lower. Thus we subsequently fit a power law to only the low force data ($f < f_{c0}^{ref}$, where f_{c0}^{ref} is the estimate of f_c^{ref} from the first fit). This produces a better estimate of γ, which we then use for a second fit. This second piecewise fit gives the final value of f_c^{ref}. Fits to reference curves are shown in Fig. 11, with fit parameters γ and f_c^{ref} listed in the caption (see also Tables V, VI, and VII).

We must verify the robustness of the piecewise fitting method before interpreting the values of f_c^{ref}. Additionally, as discussed above, the co-fitting procedure itself can fail when curves do not contain a clear crossover. To validate both aspects of our procedure (piecewise fitting to reference curves and co-fitting across salt), we confirm that our results are not sensitive to the choice of reference salt concentration.

3. Choice of reference salt conditions

To explore sensitivity to the choice of reference curve, we repeat the co-fitting procedure with different choices of I_{ref}. We find that for reference curves at moderate salt conditions (20–50 mM), the results are consistent on all PEs. However, a very high salt reference curve (≈500 mM) will impede cofitting on the very flexible NAs. These findings are shown in Fig. 13 and Tables V, VI, VII, which list f_c^{ref} and α from analyses using different reference

I_{ref} (mM)	n	$[\bar{f}_0, \bar{L}_0]$	γ	f_c^{ref} (pN)	α
24	31	[1.3 1.3e-3], $I < 4$ mM	0.59	0.46 ± 0.01	0.73 ± 0.02
		[1.1 1.1e-3], 4 mM $< I <$ 10 mM			
		[1.0 1.0e-3], $I > 10$ mM			
54	13	[1.0 1.0e-3]	0.62	0.50 ± 0.01	0.71 ± 0.02
504	5	[1.2 1.0e-3], $I < 20$ mM	0.72	0.51 ± 0.01	0.73 ± 0.02
		[1.0 1.0e-3], $I > 20$ mM			

TABLE V. Co-fitting HA data using different reference curves. For each choice of I_{ref}, we list the number of curves n averaged to make the reference curve, the initial guess of $[\bar{f}_0, \bar{L}_0]$ used for co-fitting, the best-fit exponent γ for the reference curve at low forces, and α obtained from co-fitting the full data set.

curves. These tables also list the initial guess conditions used to co-fit to all reference curves. Even in cases for which a clear crossover is present, careful choice of initial conditions is required.

For HA, choice of reference curve has essentially no impact on fit α (Table V), and the data referenced to different curves collapse as expected when divided by f_c^{ref} (Fig. 13). This robustness is not surprising; depending on salt, HA's crossover force is ∼0.1–1 pN, within the scope of the force-extension curves. We note HA's l_p plateaus to its intrinsic value at around 50–100 mM and is not strongly sensitive to salt changes above 10s of mM; this explains the lack of difference in f_c^{ref}.

For ssDNA, not all choices of f_c^{ref} are equivalent. We compare co-fitting on reference curves at 54 mM and 504 mM. In this regime, ssDNA is still strongly salt sensitive, and as expected, f_c^{ref} varies greatly between the conditions. However, at 500 mM, ssDNA barely accesses the high force regime, so it is unlikely that the piecewise fitting will perform well. Further, the low salt data could not be properly co-fit onto the 504 mM curve due to minimal overlap. In an attempt to resolve this, we first co-fit moderate salt data ($I > 20$ mM) onto the 504 mM curve using initial guess $\bar{f}_0 = 3$, $\bar{L}_0 =$ 1e-3. Once co-fit, those shifted curves were averaged to create a continuation of the reference curve above the crossover force, approximating the missing high-force regime. The low salt ($I < 20$ mM) data were then co-fit onto the combined curve using initial guess $\bar{f}_0 = 10$, $\bar{L}_0 =$ 1.5e-3. However, even then

I_{ref} (mM)	n	$[\bar{f}_0, \bar{L}_0]$	γ	f_c^{ref} (pN)	α
54	8	[1.4 1.0e-3], $I < 100$ mM	0.57	0.64 ± 0.03	0.62 ± 0.09
		[0.5 1.0e-3], $I > 100$ mM			

TABLE VI. Co-fitting ssDNA data for $I_{ref} = 54$ mM. We list the number of curves n averaged to make the reference curve, the initial guess of $[\bar{f}_0, \bar{L}_0]$ used for co-fitting, the best-fit exponent γ for the reference curve at low forces, and α obtained from co-fitting the full data set.

I_{ref} (mM)	n	$[\bar{f}_0, \bar{L}_0]$	γ	f_c^{ref} (pN)	α
27	5	[1.0 1.0e-3], $I < 20$ mM	0.62	0.31 ± 0.01	0.68 ± 0.01
		[0.4 5.0e-4], 20 mM $< I <$ 1000 mM			
		[0.1 1.0e-4], $I > 1000$ mM			
57	4	[.01 1.0e-3], $I < 20$ mM	0.60	0.50 ± 0.01	0.70 ± 0.03
		[0.4 5.0e-4], 20 mM $< I <$ 1000 mM			
		[0.1 3.0e-4], $I > 1000$ mM			
507	6	[5.0 1.0e-3], $I < 20$ mM	0.64	1.65 ± 0.06	0.66 ± 0.02
		[1.0 1.0e-3], 20 mM $< I <$ 1000 mM			
		[0.5 5.0e-4], $I > 1000$ mM			

TABLE VII. Co-fitting ssRNA data using different reference curves. For each choice of I_{ref}, we list the number of curves n averaged to make the reference curve, the initial guess of $[\bar{f}_0, \bar{L}_0]$ used for co-fitting, the best-fit exponent γ for the reference curve at low forces, and α obtained from co-fitting the full data set.

the fits of the low salt data were very sensitive to the choice of initial guess and should be considered suspect. Fig. 13 confirms the lack of equivalence between the two reference conditions and shows larger error bars for the 504 mM reference curve, pointing to a failure of the co-fitting procedure. Due to the co-fitting failure for ssDNA at high salt and a lack of sufficient data at low salt, we report only the parameters for $I_{ref} = 54$ mM (Table VI).

We conducted the same tests with the ssRNA data (Table VII). As with the ssDNA data, co-fitting onto a very high salt reference curve appears problematic, showing a systematic divergence from the other two conditions as well as increased error bar sizes (Fig. 13). The

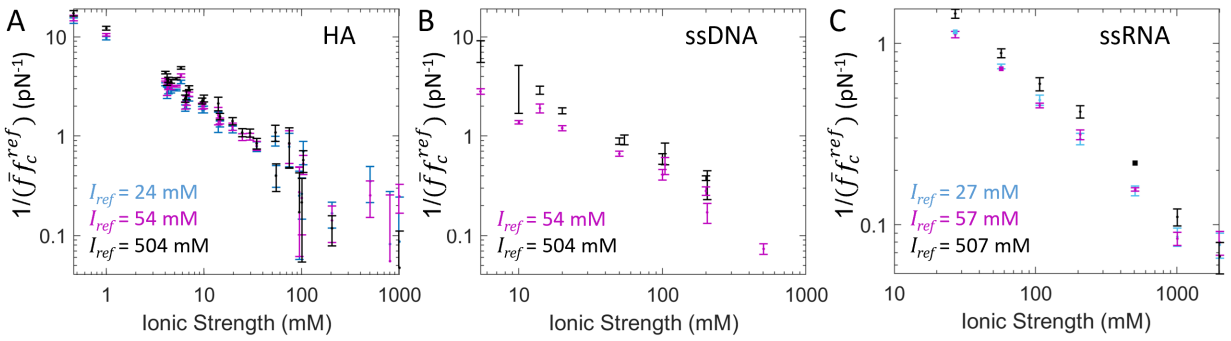

FIG. 13. Comparison of inverse crossover force values obtained from different reference curves. For HA (left), we have already subtracted the plateau value from the quantity plotted on the y-axis. Light blue: I_{ref} = 24 mM (27 mM for ssRNA), purple: I_{ref} = 54 mM (57 mM for ssRNA), black: I_{ref} = 504 mM (507 mM for ssRNA). If co-fitting procedures are equivalent, division by f_c^{ref} will collapse data referenced to different curves.

ssRNA $1/(\bar{f}f_c^{ref})$ data are consistent for the two lower-salt reference curves (27 and 57 mM), and f_c^{ref} changes are consistent with the expected salt-induced decrease in stiffness. We conclude that the co-fitting procedure is relatively robust for moderate salt reference curves.

Appendix B: Donnan Equilibrium

The Donnan equilibrium approach defines a "compartment" of volume V, containing a PE with N_0 negative charges. In the bulk, there are +1, -1, and +Z ions at concentrations c_+, c_-, and c_Z. Inside the compartment, the concentrations of each ion species are $c_{+,in}$, $c_{-,in}$, and $c_{Z,in}$. Donnan equilibrium dictates [54]:

$$\frac{c_{Z,in}}{c_Z} = \left(\frac{c_{+,in}}{c_+}\right)^Z = \left(\frac{c_{-,in}}{c_-}\right)^{-Z} \equiv g^Z. \tag{B1}$$

Charge neutrality requires:

$$Zc_{Z,in} + c_{+,in} - c_{-,in} - \frac{N_0}{V} = 0 \tag{B2}$$

inside the compartment, and

$$Zc_Z + c_+ - c_- = 0 \tag{B3}$$

outside the compartment. We rewrite the charge neutrality condition (Eq. B2) in terms of g and dimensionless parameters $p = \frac{c_+}{Zc_Z}$ and $m = \frac{N_0}{Zc_ZV}$:

$$g^{Z+1} + pg^2 - mg - (p+1) = 0. \tag{B4}$$

We then solve for g, which allows us to calculate concentrations of all species inside the cylinder, since the concentrations outside the cylinder (i.e. the bulk) are known.

ACKNOWLEDGMENTS

This work was supported by the National Science Foundation under Award 2005189. We thank I. L. Morgan for assistance in preparing DNA for these experiments. This work was performed, in part, at the Center for Integrated Nanotechnologies, an Office of Science User Facility operated for the U.S. Department of Energy (DOE) Office of Science. Sandia National Laboratories is a multimission laboratory managed and operated by National Technology & Engineering Solutions of Sandia, LLC, a wholly owned subsidiary of Honeywell International, Inc., for the U.S. DOE's National Nuclear Security Administration under contract DE-NA-0003525. The views expressed in the article do not necessarily represent the views of the U.S. DOE or the United States Government.

---

[1] R. S. Farinato, Applications of polyelectrolytes in aqueous media (ACS Publications, 2006).

[2] T. Odijk, Polyelectrolytes near the rod limit, Journal of Polymer Science: Polymer Physics Edition **15**, 477 (1977).

[3] S. Förster and M. Schmidt, Polyelectrolytes in solution, Physical Properties of Polymers , 51 (1995).

[4] J. Skolnick and M. Fixman, Electrostatic persistence length of a wormlike polyelectrolyte, Macromolecules **10**, 944 (1977).

[5] C. G. Baumann, S. B. Smith, V. A. Bloomfield, and C. Bustamante, Ionic effects on the elasticity of single dna molecules, Proceedings of the National Academy of Sciences **94**, 6185 (1997).

[6] A. Savelyev, Do monovalent mobile ions affect dna's flexibility at high salt content?, Physical Chemistry Chemical Physics **14**, 2250 (2012).

[7] A. Brunet, C. Tardin, L. Salome, P. Rousseau, N. Destainville, and M. Manghi, Dependence of dna persistence length on ionic strength of solutions with monovalent and divalent salts: a joint theory–experiment study, Macromolecules **48**, 3641 (2015).

[8] S. Guilbaud, L. Salomé, N. Destainville, M. Manghi, and C. Tardin, Dependence of dna persistence length on ionic strength and ion type, Physical review letters **122**, 028102 (2019).

[9] B. Tinland, A. Pluen, J. Sturm, and G. Weill, Persistence length of single-stranded dna, Macromolecules **30**, 5763 (1997).

[10] O. A. Saleh, D. McIntosh, P. Pincus, and N. Ribeck, Nonlinear low-force elasticity of single-stranded dna molecules, Physical review letters **102**, 068301 (2009).

[11] D. McIntosh and O. A. Saleh, Salt species-dependent electrostatic effects on ssdna elasticity, Macromolecules **44**, 2328 (2011).

[12] D. R. Jacobson, D. B. McIntosh, and O. A. Saleh, The snakelike chain character of unstructured rna, Biophysical Journal **105**, 2569 (2013).

[13] A. Bosco, J. Camunas-Soler, and F. Ritort, Elastic properties and secondary structure formation of single-stranded dna at monovalent and divalent salt conditions, Nucleic acids research **42**, 2064 (2014).

[14] J. P. Berezney and O. A. Saleh, Electrostatic effects on the conformation and elasticity of hyaluronic acid, a moderately flexible polyelectrolyte, Macromolecules **50**, 1085 (2017).

[15] J.-L. Barrat and J.-F. Joanny, Persistence length of polyelectrolyte chains, EPL (Europhysics Letters) **24**, 333 (1993).

[16] W. F. Reed, S. Ghosh, G. Medjahdi, and J. Francois, Dependence of polyelectrolyte apparent persistence lengths, viscosity, and diffusion on ionic strength and linear charge density, Macromolecules **24**, 6189 (1991).

[17] N. Grønbech-Jensen, R. J. Mashl, R. F. Bruinsma, and W. M. Gelbart, Counterion-induced attraction between rigid polyelectrolytes, Physical Review Letters **78**, 2477 (1997).

[18] G. S. Manning, Limiting laws and counterion condensation in polyelectrolyte solutions i. colligative properties, The journal of chemical Physics **51**, 924 (1969).

[19] F. Oosawa, Polyelectrolytes. (M. Dekker, New York, 1971).

[20] G. S. Manning, Limiting laws and counterion condensation in polyelectrolyte solutions: Iv. the approach to the limit and the extraordinary stability of the charge fraction, Biophysical chemistry **7**, 95 (1977).

[21] G. S. Manning, The molecular theory of polyelectrolyte solutions with applications to the electrostatic properties of polynucleotides, Quarterly reviews of biophysics **11**, 179 (1978).

[22] Y. Burak, G. Ariel, and D. Andelman, Competition between condensation of monovalent and multivalent ions in dna aggregation, Current opinion in colloid & interface science **9**, 53 (2004).

[23] A. V. Dobrynin, Effect of counterion condensation on rigidity of semiflexible polyelectrolytes, Macromolecules **39**, 9519 (2006).

[24] M. Deserno, C. Holm, and S. May, Fraction of condensed counterions around a charged rod: Comparison of poisson- boltzmann theory and computer simulations, Macromolecules **33**, 199 (2000).

[25] M. Deserno and C. Holm, Cell model and poisson-boltzmann theory: a brief introduction, in Electrostatic effects in soft matter and biophysics (Springer, 2001) pp. 27–52.

[26] B.-Y. Ha and A. J. Liu, Counterion-mediated attraction between two like-charged rods, Physical Review Letters **79**, 1289 (1997).

[27] M. Muthukumar, Theory of counter-ion condensation on flexible polyelectrolytes: Adsorption mechanism, The Journal of chemical physics **120**, 9343 (2004).

[28] R. Golestanian, M. Kardar, and T. B. Liverpool, Collapse of stiff polyelectrolytes due to counterion fluctuations, Physical review letters **82**, 4456 (1999).

[29] F. J. Solis and M. O. de la Cruz, Collapse of flexible polyelectrolytes in multivalent salt solutions, The Journal of Chemical Physics **112**, 2030 (2000), https://doi.org/10.1063/1.480763.

[30] D. M. Rose, M. Bleam, M. Record, and R. Bryant, 25mg nmr in dna solutions: dominance of site binding effects, Proceedings of the National Academy of Sciences **77**, 6289 (1980).

[31] W. H. Braunlin and Q. Xu, Hexaamminecobalt(iii) binding environments on double-helical dna, Biopolymers **32**, 1703 (1992), https://onlinelibrary.wiley.com/doi/pdf/10.1002/bip.360321212.

[32] D. B. McIntosh, G. Duggan, Q. Gouil, and O. A. Saleh, Sequence-dependent elasticity and electrostatics of single-stranded dna: signatures of base-stacking, Biophysical journal **106**, 659 (2014).

[33] D. R. Jacobson, D. B. McIntosh, M. J. Stevens, M. Rubinstein, and O. A. Saleh, Single-stranded nucleic acid elasticity arises from internal electrostatic tension, Proceedings of the National Academy of Sciences **114**, 5095 (2017).

[34] S. N. Innes-Gold, P. A. Pincus, M. J. Stevens, and O. A. Saleh, Polyelectrolyte conformation controlled by a trivalent-rich ion jacket, Physical review letters **123**, 187801 (2019).

[35] R. R. Netz and H. Orland, Variational charge renormalization in charged systems, The European Physical Journal E **11**, 301 (2003).

[36] E. Fouissac, M. Milas, M. Rinaudo, and R. Borsali, Influence of the ionic strength on the dimensions of sodium hyaluronate, Macromolecules **25**, 5613 (1992).

[37] J. C. Salamone, Polymeric materials encyclopedia, Twelve volume set (CRC press, 1996).

[38] M. van den Hout, G. M. Skinner, S. Klijnhout, V. Krudde, and N. H. Dekker, The passage of homopolymeric rna through small solid-state nanopores, Small **7**, 2217 (2011), https://onlinelibrary.wiley.com/doi/pdf/10.1002/smll.201100265.

[39] T. Strick, J.-F. Allemand, D. Bensimon, and V. Croquette, Behavior of supercoiled dna, Biophysical Journal **74**, 2016 (1998).

[40] N. Ribeck and O. A. Saleh, Multiplexed single-molecule measurements with magnetic tweezers, Review of Scientific Instruments **79**, 094301 (2008), https://aip.scitation.org/doi/pdf/10.1063/1.2981687.

[41] B. M. Lansdorp and O. A. Saleh, Power spectrum and allan variance methods for calibrating single-molecule video-tracking instruments, Review of Scientific Instruments **83**, 025115 (2012), https://doi.org/10.1063/1.3687431.

[42] C. Gosse and V. Croquette, Magnetic tweezers: micromanipulation and force measurement at the molecular level, Biophysical journal **82**, 3314 (2002).

[43] B. M. Lansdorp, S. J. Tabrizi, A. Dittmore, and O. A. Saleh, A high-speed magnetic tweezer beyond 10,000 frames per second, Review of Scientific Instruments **84**, 044301 (2013), https://doi.org/10.1063/1.4802678.

[44] M. J. Stevens and O. A. Saleh, Simulations of stretching a flexible polyelectrolyte with varying charge separation, The European Physical Journal Special Topics **225**, 1683 (2016).

[45] M. J. Stevens, J. P. Berezney, and O. A. Saleh, The effect of chain stiffness and salt on the elastic response of a polyelectrolyte, The Journal of Chemical Physics **149**, 163328 (2018), https://doi.org/10.1063/1.5035340.

[46] R. L. Cleland, J. L. Wang, and D. M. Detweiler, Polyelectrolyte properties of sodium hyaluronate. 2. potentiometric titration of hyaluronic acid, Macromolecules **15**, 386 (1982).

[47] H. V. Annapureddy and L. X. Dang, Molecular mechanism of specific ion interactions between alkali cations and acetate anion in aqueous solution: a molecular dynamics study, The Journal of Physical Chemistry B **116**, 7492 (2012).

[48] T. Sun, A. Mirzoev, N. Korolev, A. P. Lyubartsev, and L. Nordenskiold, All-atom md simulation of dna condensation using ab initio derived force field parameters of cobalt (iii)-hexammine, The Journal of Physical Chemistry B **121**, 7761 (2017).

[49] P. Pincus, Excluded volume effects and stretched polymer chains, Macromolecules **9**, 386 (1976).

[50] R. R. Netz, Strongly stretched semiflexible extensible polyelectrolytes and dna, Macromolecules **34**, 7522 (2001).

[51] D. R. Jacobson, Electrostatics of single-stranded nucleic acids: Force spectroscopy and ion counting experime Ph.D. thesis, University of California, Santa Barbara (2016).

[52] M. A. Napier and N. M. Hadler, Effect of calcium on structure and function of a hyaluronic acid matrix: carbon-13 nuclear magnetic resonance analysis and the diffusional behavior of small solutes, Proceedings of the National Academy of Sciences **75**, 2261 (1978).

[53] R. A. Robinson and R. H. Stokes, Electrolyte solutions (Courier Corporation, 2002).

[54] F. G. Donnan, The theory of membrane equilibria., Chemical reviews **1**, 73 (1924).

[55] A. L. R. Mercê, L. C. M. Carrera, L. K. S. Romanholi, and M. Á. L. Recio, Aqueous and solid complexes of iron (iii) with hyaluronic acid: Potentiometric titrations and infrared spectroscopy studies, Journal of inorganic biochemistry **89**, 212 (2002).

[56] H. Lodish, A. Berk, S. L. Zipursky, P. Matsudaira, D. Baltimore, and J. Darnell, Intracellular ion environment and membrane electric potential, in Molecular Cell Biology. 4th edition (WH Freeman, 2000).

[57] K. Bradshaw and M. Smith, Disorders of sodium balance after brain injury, Continuing Education in Anaesthesia, Critical Care & Pain **8**, 129 (2008).

[58] W. Jahnen-Dechent and M. Ketteler, Magnesium basics, Clinical kidney journal **5**, i3 (2012).

[59] M. Parikh and S. T. Webb, Cations: potassium, calcium, and magnesium, Continuing Education in Anaesthesia, Critical Care & Pain **12**, 195 (2012).